Comparative EPMA and μ-XRF methods for mapping micro-scale distribution of iodine in biocarbonates of the Callovian-Oxfordian clayey formation at Bure, Eastern part of the Paris Basin

Catherine Lerouge, Francis Claret, M.A. Denecke, Guillaume Wille, G. Falkenberg, Claire Ramboz, Claire Bény, Eric Giffaut, T. Schäfer, Eric C. Gaucher, et al.

Comparative EPMA and μ-XRF methods for mapping micro-scale distribution of iodine in biocarbonates of the Callovian–Oxfordian clayey formation at Bure, Eastern part of the Paris Basin

C. Lerouge[a] F. Claret[a], M.A. Denecke[b], G. Wille[a], G. Falkenberg[c], C. Ramboz[d], C. Beny[a], E. Giffaut[e], T. Schäfer[b, f], E.C. Gaucher[a], C. Tournassat[a]

[a] BRGM, BP36009, 45060 Orléans cédex 02, France

[b] Karlsruhe Institute of Technology (KIT) – Campus Nord, Institut Nukleare Entsorgung, Post Box 3640, 76021 Karlsruhe, Germany

[c] Hamburger Synchrotronstrahlungslabor HASYLAB at Deutschen Elektronen-Synchrotron (DESY), Notkestrasse 85, 22603 Hamburg, Germany

[d] Institut des Sciences de la Terre d'Orléans (ISTO) – CNRS, 1A rue de la Ferollerie, 45071 ORLEANS Cedex 2, France

[e] ANDRA, 92298 Châtenay-Malabry Cedex, France

[f] Institute of Geological Sciences, Department of Earth Sciences, Freie Universität Berlin, Berlin, Germany

Abstract

A pluridisciplinary approach was used to define iodine immobilization mechanisms by biocarbonates in a natural marine carbonate-bearing clayey formation. For this purpose, different techniques of observation (optical microscope, scanning electron microscope (SEM), cathodoluminescence (CL)) and of analyses (infrared spectrometry (IR), electron microprobe (EPMA), spatially resolved synchrotron-based X-ray fluorescence (μ-XRF) and X-ray diffraction (μ-XRD)) were performed on two entire and centimeter-sized carbonate shells of the Callovian–Oxfordian (160 Ma) clayey formation from the ANDRA (French Radioactive Waste Management Agency) Underground Research Laboratory (Meuse/Haute Marne, France), in the Eastern part of the Paris Basin. Combined (SEM, CL, IR and μ-XRD) data indicates that the biostructure of the Rhynchonella shell is relatively well-preserved but bio-aragonite slowly transforms into calcite, whereas the bivalve shell is entirely recrystallized into diagenetic calcite and celestite. EPMA and μ-XRF data show bioaccumulation of iodine in carbonate shells, confirming previous work on present-day mollusks. EPMA analyses give evidence of iodine content up to 1200 ppm in the preserved Rhynchonella shell and up to 2000 ppm in recrystallized bivalve shell. μ-XRF elemental mapping shows that iodine is more homogeneously distributed in bio-calcite of the Rhynchonella shell than in recrystallized calcite of the bivalve shell, suggesting a loss of iodine during re-crystallization processes, but not a total exclusion of iodine from the carbonate structure. Combined EPMA data and μ-XRF elemental maps do not give evidence of any correlation between the iodine location and the distribution of other elements.

Keywords: Iodine; Biocarbonate; EPMA; μ-XRF; Callovian–Oxfordian claystone; ANDRA

1. Introduction

The fate of [129]I, a long-lived nuclide, in underground nuclear waste disposal in clayey formations is a major concern. Indeed, in addition to its long-life period, its mobility and its ubiquity in radioactive waste, iodine [129]I will make a significant contribution to potential overall long-term dose resulting from waste storage ([Altmann, 2008] and [Grambow, 2008]). [129]I has a complex chemistry in the environment. Iodine can be found in an elemental form I_2 (valence 0), as iodide I^- (−1) or iodate IO_3^- (+5). Its fate and transport are dictated by its chemical speciation (Koch-Steindl and Prohl, 2001). Soluble iodine will probably exhibit its −1 valence state as the iodide anion (I^-) in clayey formations such as Callovian–Oxfordian (COx, France), Opalinus Clay (OPA, Switzerland) or Boom Clay (Belgium), according to the near-neutral pH and low redox potential of these media ([Appelo et al., 2008] , [Gaucher et al., 2006] , [Gaucher et al., 2009] , [18] and [Vinsot et al., 2008]). Due to the inherent negative surface charge of clay rock minerals at near neutral and basic pH conditions, I^- is repelled from their surface and generally shows an absence or even a negative adsorption (e.g. carbonates, quartz, chlorite, montmorillonite and muscovite, see Tournassat et al. (2007) and references therein, and illite, Montavon et al. (2009)). Paradoxically, up to now diffusion transport experiments have systematically shown a low but significant retardation factor for iodine transport in comparison to the Cl as conservative tracer. Recent experiments by Glaus et al. (2008) have lent a clearer view of processes occurring during diffusion experiments showing that most probably this retardation can be attributed to a small amount of iodate in the radiotracers used to performed the diffusion experiments.

The results from Glaus et al. (2008) also highlight the need to understand natural iodine behaviour in clay rock systems, because [129]I associated with nuclear waste is expected to exhibit geochemical behaviour the same as natural isotopes. This has been tackled by Claret et al. (2010) by characterizing the different iodine reservoirs in Callovian–Oxfordian clayey formation of Bure. In that study, sequential chemical extraction data have shown that ~66% of the low iodine content of the claystone (1–5 ppm) is associated with the carbonate fraction and ~33% with organic matter. This surprising finding was confirmed by electron microprobe analyses (EPMA) that have been performed on detrital and different generations of diagenetic carbonates identified in thin sections and described in Tournassat et al. (2008). These analyses have provided evidence of low and heterogeneously distributed iodine contents measured in bioclasts of bivalves and brachiopods (Rhynchonella and Terebratula) (up to 1300 ppm), but also in less amounts in diagenetic euhedral calcite and dolomite (up to 620 ppm). However EPMA analyses to measure iodine is especially challenging due to spectral interference between calcium K and iodine L emission lines and to the relatively high detection limits (~150 ppm). As a consequence it was necessary to confirm these results with another spectroscopic technique. We therefore applied spatially resolved synchrotron-based X-ray fluorescence (μ-XRF) using a micro-focused beam at energies above the I K absorption to excite I Kα fluorescence in the present study. Following previous findings in Claret et al. (2010) the investigations were conducted on carbonate shells of mollusk bivalve and brachiopod (Rhynchonella) originating from the Callovian–Oxfordian clayey formation (~160 Ma), in an attempt to define the iodine speciation and immobilization mechanisms by carbonates in a natural carbonate-bearing clayey formation. μ-XRF analyses combined with other techniques (EPMA, microscopy, cathodoluminescence) were performed, in order to ascertain element/mineral distribution correlations.

2. Material and methods

2.1. Material

Entire and centimeter-sized shells of an undetermined mollusk bivalve and a brachiopod (Rhynchonella), were separated by handpicking in a claystone sample from gallery level of the ANDRA underground research laboratory (URL) at Bure (Meuse–Haute-Marne, France). They were cut along two perpendicular directions to obtain 60–70 μm-thick polished sections of the shells. A dry polishing procedure was performed to avoid any partial dissolution of calcite and done by hand to avoid any heating and volatilization of iodine.

2.2. Scanning electron microscope

Observations, analyses and elemental mapping were performed with a JEOL JSM 6100 scanning electron microscope (SEM) coupled with an energy dispersive spectrometer (Kevex Quantum) at 25 kV. Prior to analysis, a 10–20 nm thick carbon layer was sputter-coated on the samples (Edwards Auto 306).

2.3. Cathodoluminescence

Cathodoluminescence (CL) was used to identify Ca-carbonate polymorphs (aragonite and calcite) and to distinguish carbonate biomineralization and diagenetic calcite. The luminescence characteristics of carbonate minerals are controlled by the relative abundances of rare earth elements (REE), manganese and iron. Mn^{2+} ion and trivalent REE ions appear to be the most important activator ions of extrinsic CL, whereas Fe^{2+} is the main quencher ([15] and [Richter et al., 2003]). The most common extrinsic colors of calcite and aragonite are, respectively, yellow–orange to orange and yellow–green to green. As a consequence, CL measurements enable to distinguish easily these two polymorphs of $CaCO_3$. The system used was a cold cathode Cathodyne from OPEA Society (*Laboratoire Optique Electronique Appliquée*). The electron beam has adjustable energies up to 26 keV and currents up to 250 μA. The cathodyne is mounted on a Olympus microscope allowing magnification up to 10×. The system is equipped with a JVC KY-F75U tri-CCD digital camera. The three 12 mm-sized sensors have a resolution of 1360×1024 pixels.

2.4. Infra-red absorbance

Infrared spectra were obtained with an attenuated total reflection (ATR) cell (Golden Gate) on a Bruker Equinox IFS-55 infrared spectrometer. Twenty scans were performed for each spectrum from 4000 to 550 cm^{-1}, with a spectral resolution of 4 cm^{-1}.

2.5. Electron microprobe

EPMA analyses were performed on the polished thin sections using a Cameca SX50 electron microprobe with a 20 kV acceleration voltage, a current beam of 50 nA and a 1–2 μm beam width. Prior to analysis, a 10–20 nm thick carbon layer was sputter-coated on the samples (Edwards Auto 306). Ca, Fe, Mg, S and Sr elements were analysed simultaneously with iodine. Ca Lα, S Kα and I Lβ were analyzed using a PET (Pentaerythritol) crystal. Fe Kα was analyzed using a LiF (Lithium fluoride) crystal. Mg Kα and Sr Kα were analyzed using a TAP (Thallium acid phthalate) crystal. Standards used included both well-characterized natural minerals: apatite for Ca and P, barytine for Ba and S, olivine for Mg, $SrSO_4$ for S, and synthetic Fe_2O_3 for Fe. Iodine standard is synthetic $Bi_{19}I_3S_{27}$ ([Devic et al., 2003] and

[Doussier et al., 2007]). Counting times were 40 s for Ca, S, Fe, Mg, Sr, and P, and 240 s for I. Matrix corrections were made with a ZAF computing program (Sweatman and Long, 1969).

2.6. Micro-X-ray fluorescence

The μ-XRF experiments were performed at Beamline L of the DORIS III synchrotron ring, which is operated by the Hamburg Synchrotron Radiation Laboratory HASYLAB at the German Electron Synchrotron DESY (Hamburg, Germany) ([7] and [8]). A band pass of energies with a narrow wavelength range centered at 0.34 Å was selected from the white beam from a bending magnet using a NiC multilayer monochromator. The incident radiation was focused with an elliptical single-bounce monocapillary to deliver a footprint on the sample approximately 15 μm diameter at 45° orientation of the sample to the incident beam. The sample is mounted on an x, y positioning stage to scan in a step-by-step (i.e., pixel by pixel) fashion over selected sample areas. The X-ray microbeam was focused to the focal plan of the optical microscope used for on-line visualization of the sample. A high resolution CCD camera (MAR CCD, MARUSA Co.) was placed 27.3 cm behind the sample for registering XRD diffractograms at each pixel using 5 s illumination times. The XRD geometry was calibrated using a LaB_6 powder standard. The fluorescence emitted by the sample was detected at an angle of 90° to the incoming beam using two successive detectors: a Si-drift detector (Vortex, SII Technologies Inc.) and a Si(Li) detector (Gresham Scientific Instruments Ltd.) having a 400 μm-Al filter. Two-dimensional X-ray intensity maps were obtained using a 10 s acquisition time for each pixel. X-ray spectra of each pixel were evaluated by non-linear least-square fits using the AXIL software package (Vekemans et al., 1994). Elemental distribution maps for Ca, Fe, Mn, S, Sr, Ba, Sn and I are obtained by plotting background corrected fluorescence intensities for Ca Kα, Fe Kα, Mn Kα, Sr Kα, Ba Kα, Sn Kα and I Kα/Lα as a function of pixel position of the area scanned. The intensities are scaled in shades of black, grey, and white by assigning the pixel with the largest corresponding fluorescence intensity signal the color black, the pixel with the lowest intensity white, and scaling the remaining pixel intensities accordingly on a relative linear scale.

3. Results

3.1. Microscopic observations, infrared spectrometry and μ-XRD

Optical microscope, SEM, cathodoluminescence (CL) images and infrared spectrometry results for both bioclasts are depicted in Fig. 1A–C. The one dimensional μ-XRD isolated for a 80×80 μm^2 area on the bivalve shell is displayed in Fig. 1D.

The Rhynchonella shell shows well-preserved bio-organic structures visible in the optical microscope, SEM and CL images. CL image of shell reveals dark orange calcite with green micro-inclusions of aragonite, indicating that shell consist of calcite likely resulting from the slow transformation of bio-aragonite. No celestite inclusion was observed. Infrared spectrometry confirms that calcium carbonate is dominantly calcite (peaks at ~712, ~871 and ~1388 cm^{-1}) with traces of aragonite revealed by the form of the spectra in the range of 1500–1400 cm^{-1} and the width of the peak at ~840–880 cm^{-1} (Compere and Bates, 1973).

The bivalve shell does not exhibit any organic structures and contains some 100 μm-sized inclusions of celestite [$SrSO_4$] observed in transmitted light. SEM images provide also evidence of numerous micro-sized inclusions of celestite that were not observed with optical microscope. CL image of shell reveals recrystallized zoned orange calcite. Infrared

spectrometry confirms that the calcium carbonate is dominantly calcite, probably with residual aragonite. The μ-XRD diffractogram shows peaks at positions expected for calcite (Maslen et al., 1993) but with different intensities than expected for a non-oriented powder pattern, suggesting that the calcite crystals in the shell likely have a preferred orientation.

The combined data indicates that the biostructure of the Rhynchonella shell is relatively well-preserved but bio-aragonite slowly transforms into calcite, whereas the bivalve shell is entirely recrystallized into diagenetic calcite and celestite.

3.2. EPMA analyses

One hundred EPMA automatic analyses were performed along five transections in the well-preserved bio-aragonite of the Rhynchonella shell and along seven transections in the recrystallized calcite of the bivalve shell. The impact of the electron beam was larger in bio-aragonite (∼12–15 μm sized craters) than in recrystallized calcite (∼2 μm), indicating a lower hardness of biocarbonate than recrystallized calcite (Fig. 2). In both bioclasts, iodine occurs heterogeneously distributed in the shell with 17% of the values measured for the Rhynchonella shell and 32% of values for the bivalve shell lying above the detection limit (200 ppm). Four and 8% of measured values for Rhynchonella and bivalve shells, respectively, are above 1000 ppm, i.e., 5× detection limit, and represent significant values (Table 1). Principal Components Analysis (PCA) treatment of the data does not give evidence of any correlation of iodine with other trace elements.

3.3. μ-XRF mapping

The XRF spectra measured with the Si-drift detector provide evidence of Fe, Mn, S, Sn, Sr in Ca carbonates of both types of bioclasts studied. Elemental distribution maps (20 μm step size) for iodine and other detected elements for a 420 μm × 620 μm area of the polished section of well-preserved Rhynchonella shell and for a 360 μm × 280 μm of the polished section of recrystallized bivalve shell are shown in Fig. 3.

The bottom left corner of the maps for the Rhynchonella shell corresponds to zones previously analyzed by electron microprobe and can be identified on the maps by light zones in the maps where elements were volatized. Elsewhere in the area studied Fe is localized in the lower right corner and the Mn distribution is generally homogeneous and negatively correlated to the Ca distribution. Sr and Ba occur as two small (approximately 100 μm) dark areas. Noticeable in the data collected with the Si-drift detector for both shells is the difference between I Lα and I Kα maps. The I Lα intensities have obviously not been sufficiently separated from the Ca Kα emission lines, as the I Lα map correspond well to the Ca distribution. The I Kα map shows a homogeneous distribution of iodine in the well-preserved Rhynchonella shell.

The element distribution maps of the bivalve shell show that calcite (Ca-rich dark zones in the Ca map) has homogeneous Mn content and a low but also homogeneous distribution of Fe. The calcite is bordered by associated Sr-rich (Ca-free) zones indicating the presence of celestite ($SrSO_4$), intimately associated with Ba traces. The I Kα map provides evidence of global low iodine content and a very heterogeneous distribution of iodine in recrystallized calcite. Iodine is not detected in Sr-rich celestite.

An important constraint of the experiment made these measurements especially challenging. The energy of the Sr Kα emission line (∼14.1 keV) is nearly half that of the energy of I Kα lines (28.6 and 28.3 keV). This means that the occurrence of spectral sum peaks or the simultaneous detection of two strontium quanta (pulse pile-up in the detector) will be counted as an I Kα emission and lead to a source of error. In addition, high background levels and broad peak widths are not conducive for detection of trace species. In order to optimize experimental conditions to minimize the effects of these constraints, the μ-XRF data was re-collected using a Si(Li) detector with a 400 μm-Al filter. This decreases the incoming total count rate, pile up and peak broadening. The advantage of this strategy is demonstrated in Fig. 4. An improvement in background and counting statistics allows obtaining better spectra. However the intensity of the I Kα remained low, rendering quantification of iodine in these measurements difficult. A qualitative comparison is possible, however. The superposition of spectra from the both shell types studied shows that the iodine peak (and consequently iodine content) is higher in the Rhynchonella shell than in the bivalve shell (Fig. 4). The elemental distribution maps for Sr, Ba, Sn and I using the Si(Li) detector with 400 μm-Al filter are comparable to the elemental maps recorded using the Si-drift detector (Fig. 3).

4. Discussion-conclusion

This work shows bioaccumulation of iodine in carbonate shells, confirming reports from previous work on present-day mollusks (Ishii, 1997). The iodine content measured by EPMA is up to 1200 ppm in the preserved Rhynchonella shell and up to 2000 ppm in the bivalve shell. In contrast, the relative iodine content measured by synchrotron-based μ-XRF is higher in the Rhynchonella shell than in the bivalve calcite shell.

Unfortunately, combined EPMA data and μ-XRF elemental maps did not give evidence of any correlation between iodine location and the distribution of other elements. These EPMA and μ-XRF studies illustrate the experimental challenges in measuring iodine in calcium carbonates. The contrast in results of iodine content obtained by both methods could be due: (1) to the different hardness of biocarbonates included in an organic structure and chemical calcite (cf. Fig. 2), (2) to the difference in sensitivities of the two analytical techniques, and/or (3) to the inhomogeneity of iodine concentrations in the samples that was evidenced during this work.

Diagenesis has induced partial to total in situ re-crystallization of aragonite and bio-calcite into diagenetic carbonates, dissolution of biocarbonates and precipitation of diagenetic carbonates in the Callovian–Oxfordian clayey formation under reducing conditions. According to these μ-XRF data, iodine is more homogeneously distributed in bio-calcite of the Rhynchonella shell than in recrystallized calcite of the bivalve shell. This suggests a loss of iodine during the re-crystallization processes, but not a total exclusion of iodine from the carbonate structure. We cannot differentiate if the homogenous distribution of iodine in the Rhynchonella inhibits the re-crystallization process or simply results from the presence of biological organic structures with high calcite content. Rough calculation made by Claret et al. (2010) rather suggests that iodine is not associated to organic incorporated in the carbonate structure and therefore favor re-crystallisation process.

These results and small localized iodine contents observed in diagenetic euhedral calcite and dolomite could point to a mechanism of partial immobilization of iodine liberated from bioclast dissolution by incorporation into diagenetic carbonates during diagenesis of the clay sediment.

Despite this new confirmation of iodine/carbonate association, precise determination of the iodine speciation (I^-, IO_3^-, I_2 or organic iodine) in these minerals remains unresolved at this stage of the study. The measurement of near edge absorption spectra for iodine is proved difficult because the most intense iodine Lα X-ray emissions lines are masked by calcium X-rays lines. Measurement at the I Kα edge can avoid spectral interference but remains challenging due to the low iodine content in the carbonates and its varying distribution, especially in the bivalve shell.

Acknowledgments

References

Altmann, 2008 S. Altmann, 'Geo'chemical research: a key building block for nuclear waste disposal safety cases. *Journal of Contaminant Hydrology*, **102** (2008), pp. 174–179.

Appelo et al., 2008 C.A.J. Appelo, A. Vinsot, S. Mettler and S. Wechner, Obtaining the porewater composition of a clay rock by modeling the in- and out-diffusion of anions and cations from an in-situ experiment. *Journal of Contaminant Hydrology*, **101** (2008), pp. 67–76.

Claret et al., 2010 F. Claret, C. Lerouge, T. Laurioux, M. Bizi, T. Conte, J.P. Ghestem, G. Wille, T. Sato, E.C. Gaucher, E. Giffaut and C. Tournassat, Natural iodine in a clay formation: implications for iodine fate in geological disposals. *Geochimica Et Cosmochimica Acta*, **74** (2010), pp. 16–29.

Compere and Bates, 1973 E.L. Compere and J.M. Bates, Determination of calcite: aragonite ratios in mollusc shells by infrared spectra. *Limnology and Oceanography*, **18** (1973), pp. 326–331.

Devic et al., 2003 T. Devic, M. Evain, Y. Moelo, E. Canadell, P. Auban-Senzier, M. Fourmigue and P. Batail, Single crystalline commensurate metallic assemblages of pi-slabs and Cdl(2)-type layers: synthesis and properties of beta-(EDT-TTF-l(2))(2)[Pb-5/6 square(1/6)l(2)](3) and beta-(EDT-TTF-l(2))(2)[Pb2/3 + xAg1/3 − 2x square(x)l(2)](3), x = 0.05. *Journal of the American Chemical Society*, **125** (2003), pp. 3295–3301

Doussier et al., 2007 C. Doussier, Y. Moelo, P. Leone, A. Meerschaut and M. Evain, Crystal structure of Pb2SbS2I3, and re-examination of the crystal chemistry within the group of (Pb/Sn/Sb-) chalcogeno-iodides. *Solid State Science*, **9** (2007), pp. 792–803.

Falkenberg et al., 2001 Falkenberg, G., Clauss, O., Tschentscher, T., 2001. X-ray Optics for the Microfocus Beamline L. HASYLAB 2001, annual report, Part 1. Available from: <http://hasylab.desy.de/science/annual_reports/2001/index_eng.html> or <http://hasyweb.desy.de/science/annual_reports/2001_report/part1/intern/5720.pdf>..

Falkenberg et al., 2003 Falkenberg, G., Rickers, K., Bilderback, D.H., Huang, R., 2003. A Single-bounce Capillary for Focusing of Hard X-rays. HASYLAB 2003, annual report, Part 1. Available from: <http://hasylab.desy.de/science/annual_reports/2003/index_eng.html>, <http://hasyweb.desy.de/science/annual_reports/2003_report/part1/intern/11062.pdf>..

Gaucher et al., 2006 E.C. Gaucher, P. Blanc, F. Bardot, G. Braibant, S. Buschaert, C. Crouzet, A. Gautier, J.-P. Girard, E. Jacquot, A. Lassin, G. Negrel, C. Tournassat, A. Vinsot and S. Altmann, Modelling the porewater chemistry of the Callovian–Oxfordian formation at a regional scale. *Comptes Rendus Geosciences*, **338** (2006), pp. 917–930.

Gaucher et al., 2009 E.C. Gaucher, C. Tournassat, F.J. Pearson, P. Blanc, C. Crouzet, C. Lerouge and S. Altmann, A robust model for pore-water chemistry of clayrock. *Geochimica et Cosmochimica Acta*, **73** (2009), pp. 6470–6487.

Glaus et al., 2008 M.A. Glaus, W. Muller and L.R. Van Loon, Diffusion of iodide and iodate through Opalinus Clay: monitoring of the redox state using an anion chromatographic technique. *Applied Geochemistry*, **23** (2008), pp. 3612–3619.

Grambow, 2008 B. Grambow, Mobile fission and activation products in nuclear waste disposal. *Journal of Contaminant Hydrology*, **102** (2008), pp. 180–186.

Ishii, 1997 T. Ishii, Specific accumulation of iodine by the operculum of the strawberry conch Strombus luhuanus. *Fisheries Science*, **63** (1997), pp. 646–647.

Koch-Steindl and Prohl, 2001 H. Koch-Steindl and G. Prohl, Considerations on the behaviour of long-lived radionuclides in the soil. *Radiation and Environmental Biophysics*, **40** (2001), pp. 93–104.

Marshall, 1988 Marshall, D.J., 1988. Cathodoluminescence of Geological Materials Unwin Hyman, Boston..

Maslen et al., 1993 E.N. Maslen, V.A. Streltsov and N.R. Streltsova, X-ray study of the electron-density in calcite, $CaCO_3$. *Acta Crystallographica Section B*, **49** (1993), pp. 636–641.

Montavon et al., 2009 G. Montavon, Z. Guo, C. Tournassat, B. Grambow and D. Le Botlan, Porosities accessible to HTO and iodide on water-saturated compacted clay materials and relation with the forms of water: a low field proton NMR study. *Geochimica Et Cosmochimica Acta*, **73** (2009), pp. 7290–7302.

Pearson et al., 2003 Pearson, F.J., Arcos, D., Boisson, J.-Y., Fernandez, A.M., Gäbler, H.-E., Gaucher, E., Gautschi, A., Griffault, L., Hernan, P., Waber, H.N., 2003. Mont Terri project – geochemistry of water in the Opalinus clay formation at the Mont Terri Rock Laboratory. In: FOWG (Ed.), Geology Series, Bern..

Richter et al., 2003 D.K. Richter, T. Gotte, J. Gotze and R.D. Neuser, Progress in application of cathodoluminescence (CL) in sedimentary petrology. *Mineralogy and Petrology*, **79** (2003), pp. 127–166.

Sweatman and Long, 1969 T.R. Sweatman and J.V.P. Long, Quantitative electron-probe microanalysis of rock-forming minerals. *Journal of Petrology*, **10** (1969), pp. 332–379.

Tournassat et al., 2007 C. Tournassat, E.C. Gaucher, M. Fattahi and B. Grambow, On the mobility and potential retention of iodine in the Callovian–Oxfordian formation. *Physics and Chemistry of the Earth, Parts A/B/C*, **32** (2007), pp. 539–551.

Tournassat et al., 2008 C. Tournassat, C. Lerouge, J. Brendlé, J.-M. Greneche, S. Touzelet, E. Blanc and E. Gaucher, Cation exchanged Fe(II) as compared to other divalent cations (Ca, Mg, Sr) in the Callovian–Oxfordian formation. Implications for porewater composition modelling. *Applied Geochemistry*, **23** (2008), pp. 641–654.

Vekemans et al., 1994 B. Vekemans, K. Janssens, L. Vincze, F. Adams and P. Vanespen, Analysis of X-ray-spectra by iterative least-squares (axil) – new developments. *X-ray Spectrometry*, **23** (1994), pp. 278–285.

Vinsot et al., 2008 A. Vinsot, S. Mettler and S. Wechner, In situ characterization of the Callovo–Oxfordian pore water composition. *Physics and Chemistry of the Earth, Parts A/B/C*, **33** (2008), pp. S75–S86
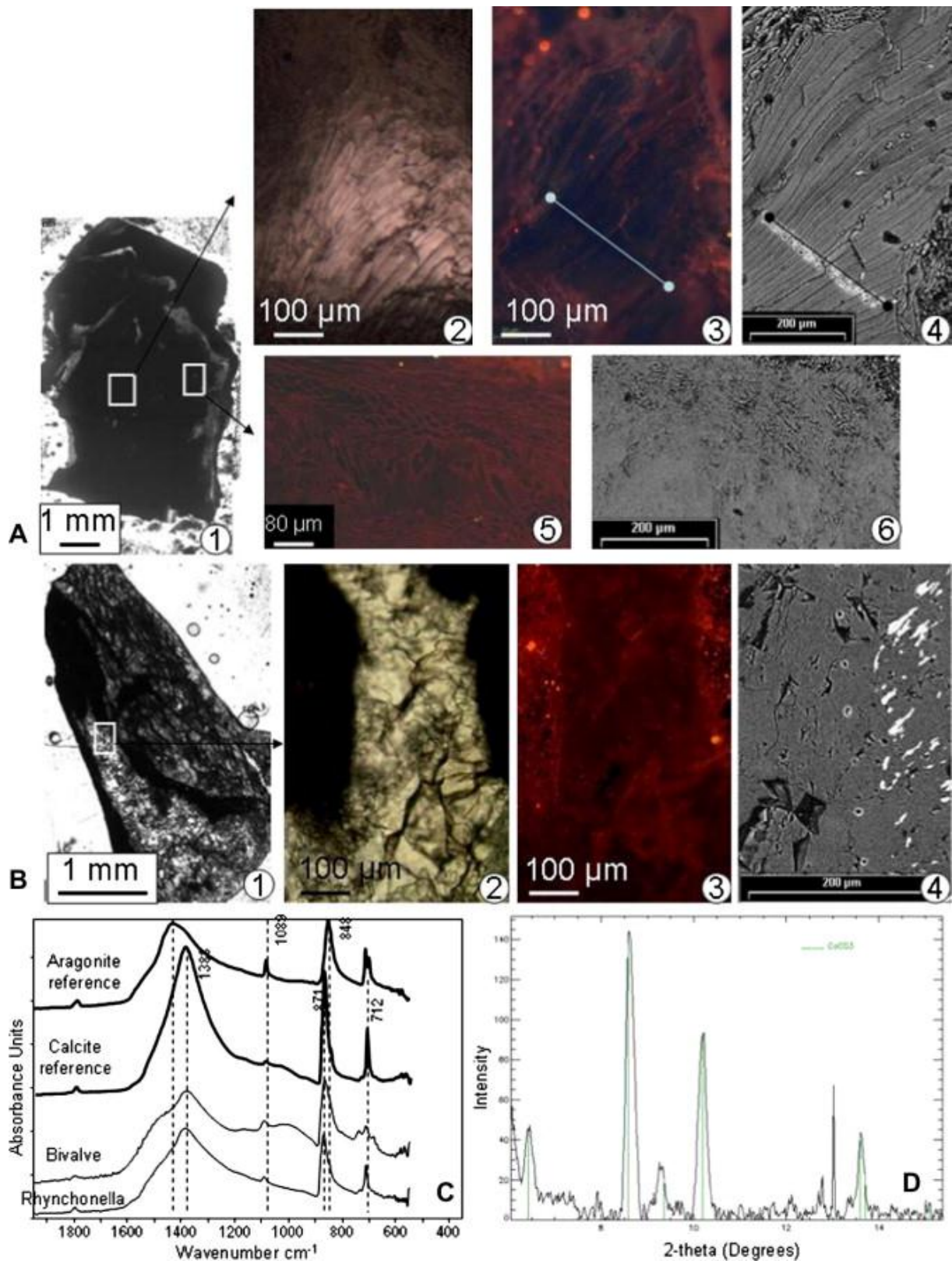
Fig. 1. : A. Rhynchonella shell: (1) optical micrograph (natural light), (2) detail SEM micrograph of the marked area in 1 showing the organic structures (parallel section), (3) corresponding cathodoluminescence image giving evidence of calcite (red color), (4) corresponding backscattered electron image, (5) cathodoluminescence image of the organic structures (perpendicular section) of the sample area indicated in 1, (6) corresponding

backscattered electron image. B. bivalve shell: (1) optical micrograph (natural light), (2) detail SEM micrograph of the marked area in 1, (3) corresponding cathodoluminescence image giving evidence of calcite (red color), (4) corresponding backscattered electron image. C. Infrared spectra of the both shells compared to aragonite and calcite references. D. μ-XRD diffraction pattern averaged over a 80 μm $\times$ 80 μm area. Vertical lines indicated expected peak positions for calcite.
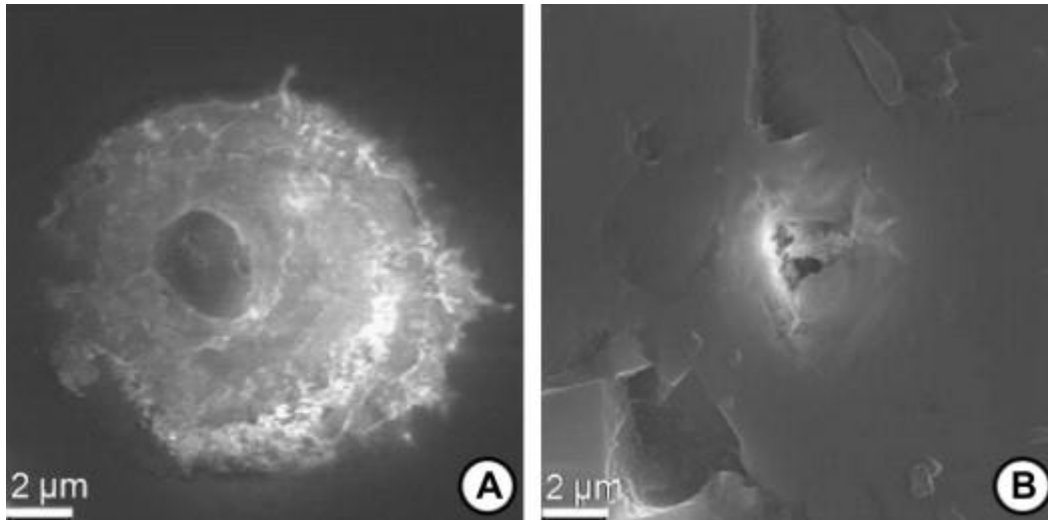
Fig. 2. : Secondary electron image showing the impact of the beam of the electron microprobe (a) in the bio-calcite of the Rhynchonella, (b) in the recrystallized calcite of the bivalve.

Table 1. Selected EPMA analyses of calcite in the well-preserved Rhynchonella shell and in the recrystallized bivalve shell. *X* is the coordinate of the analyse point in the electron microprobe, allowing to realize transection analysis or mapping. Contents of major elements: Ca, Fe and Mg, are given in weight percent of oxide. Contents of trace elements: I, Sr and S are given in ppm. A structural formula was calculated on the based of 3 oxygen atoms ($CaCO_3$).

Point	*X*	In weight% oxide				In ppm (mg/kg)			Structural formulae (three oxygens)		
		CaO	FeO	MgO	Total	I	Sr	S	Ca	Fe	Mg
EPMA analyses of the Rhynchonella shell											
101	−4284	59.95	0.04	0.14	60.13	0	879	0	0.972	0.001	0.003
102	−4276	60.38	0.05	0.34	60.77	0	550	0	0.963	0.001	0.008
103	−4269	59.12	0.04	0.18	59.34	0	719	429	0.961	0.001	0.004
104	−4262	59.69	0.15	0.11	59.94	210	727	7301	0.913	0.002	0.002
105	−4255	60.07	0.04	0.17	60.28	0	769	0	0.970	0.001	0.004
106	−4248	59.96	0.03	0.20	60.19	0	812	0	0.971	0.000	0.004
107	−4240	58.57	0.05	0.16	58.78	0	829	0	0.970	0.001	0.004
108	−4233	57.97	0.19	0.07	58.22	0	558	328	0.960	0.002	0.002
109	−4226	51.71	0.09	0.24	52.03	0	643	601	0.933	0.001	0.006
110	−4219	58.41	0.05	0.16	58.62	0	0	441	0.956	0.001	0.004
111	−4211	60.19	0.02	0.14	60.35	0	702	388	0.966	0.000	0.003
112	−4204	58.62	0.09	0.27	58.98	160	541	368	0.937	0.001	0.006
113	−4197	56.06	0.14	0.29	56.50	1030	0	489	0.907	0.002	0.007
114	−4190	60.21	0.02	0.21	60.44	0	660	368	0.958	0.000	0.005
115	−4182	61.01	0.05	0.26	61.32	0	693	521	0.960	0.001	0.006
116	−4175	56.39	0.11	0.11	56.60	1120	651	661	0.924	0.001	0.002
117	−4168	58.80	0.06	0.25	59.11	610	786	348	0.958	0.001	0.006
118	−4161	59.70	0.05	0.37	60.12	0	769	320	0.958	0.001	0.008
119	−4153	56.33	0.05	0.20	56.59	0	533	489	0.953	0.001	0.005
120	−4146	58.54	0.06	0.23	58.82	0	778	340	0.964	0.001	0.005
121	−4139	56.94	0.02	0.23	57.19	840	719	400	0.962	0.000	0.005
EPMA analyses of the recrystallized bivalve shell											
1	−942	58.92	1.61	0.63	61.57	870	3019	0	0.950	0.020	0.014
2	−935	55.73	1.22	0.82	57.90	0	781	0	0.954	0.016	0.020
3	−928	60.44	1.94	0.19	62.76	320	1267	0	0.957	0.024	0.004
4	−921	58.81	1.68	0.57	61.24	0	1499	0	0.953	0.021	0.013
5	−914	59.77	1.79	0.74	62.48	0	1288	0	0.948	0.022	0.016

| Point	X	In weight% oxide				In ppm (mg/kg)			Structural formulae (three oxygens)		
		CaO	FeO	MgO	Total	I	Sr	S	Ca	Fe	Mg
6	−907	57.26	1.69	0.47	59.59	0	887	0	0.953	0.022	0.011
7	−900	62.09	1.35	0.18	63.75	0	570	0	0.969	0.016	0.004
8	−893	61.65	2.22	0.15	64.16	1420	760	0	0.954	0.027	0.003
9	−886	59.11	2.03	0.30	61.56	0	697	0	0.953	0.026	0.007
10	−879	56.39	1.72	0.12	58.40	1750	887	0	0.960	0.023	0.003
21	−1042	62.67	0.48	0.09	63.50	0	0	1066	0.981	0.006	0.002
22	−1035	58.04	1.43	0.52	60.14	0	697	0	0.957	0.018	0.012
23	−1028	57.23	1.65	0.39	59.44	400	1098	0	0.956	0.021	0.009
24	−1021	56.78	1.91	0.80	59.62	0	802	0	0.942	0.025	0.018
25	−1014	58.85	1.53	0.10	60.77	1770	1225	530	0.963	0.020	0.002
26	−1007	54.75	1.67	0.90	57.40	0	0	0	0.943	0.022	0.022
27	−1000	58.54	2.17	0.20	61.06	2080	802	0	0.951	0.027	0.004
28	−993	59.39	2.13	1.02	62.63	340	887	0	0.937	0.026	0.022
29	−986	59.36	2.03	0.71	62.25	0	908	0	0.944	0.025	0.016
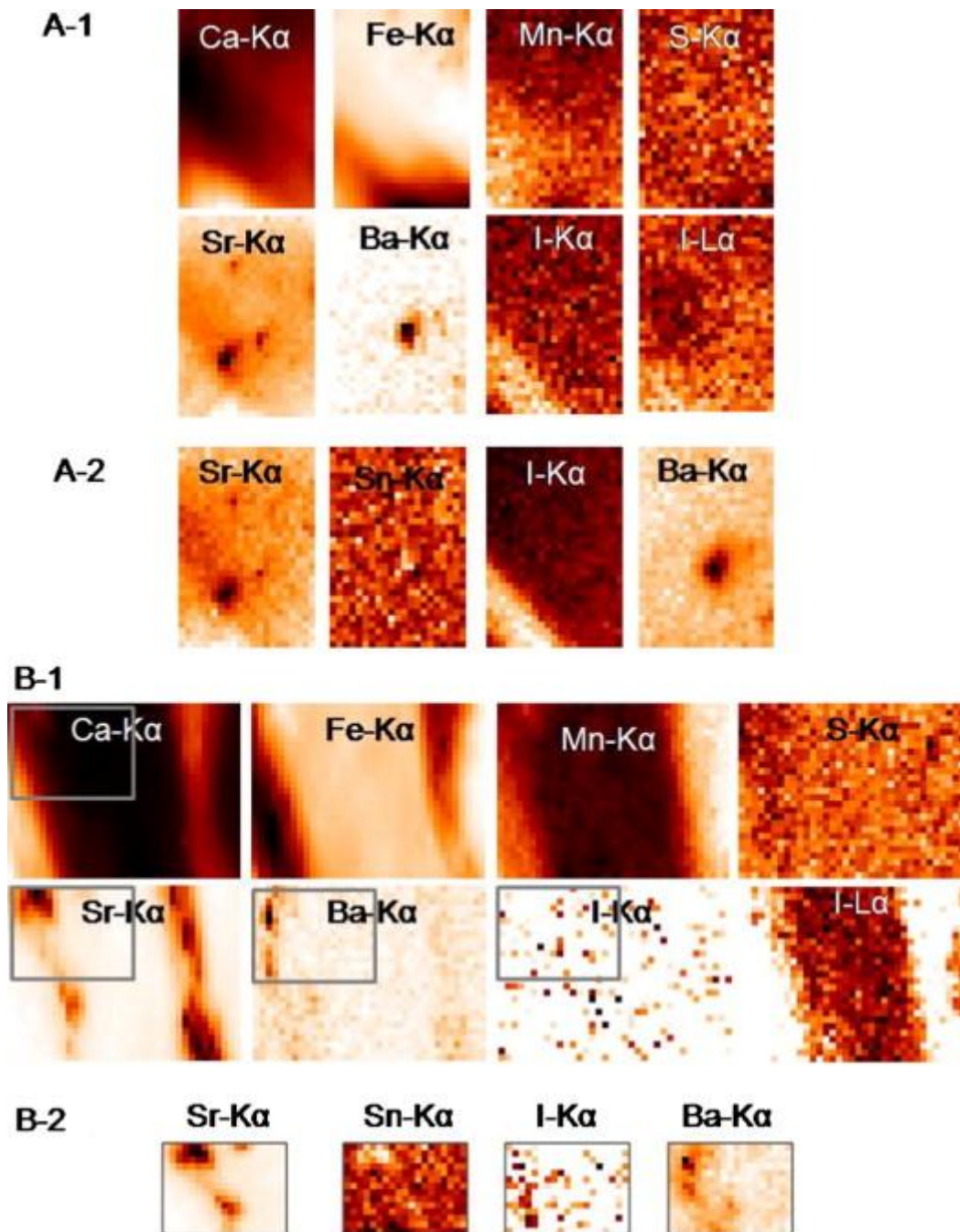
Fig. 3. : Distribution maps (20 μm pixel width) for the elements indicated as relative fluorescence intensities measured for A. bio-calcite of Rhynchonella (420 μm × 620 μm area), and B. recrystallized calcite of bivalve (360 μm × 280 μm area). 1. Maps realized using a Si-drift detector, 2. Maps realized using a Si(Li) detector with a 400 μm-Al filter.
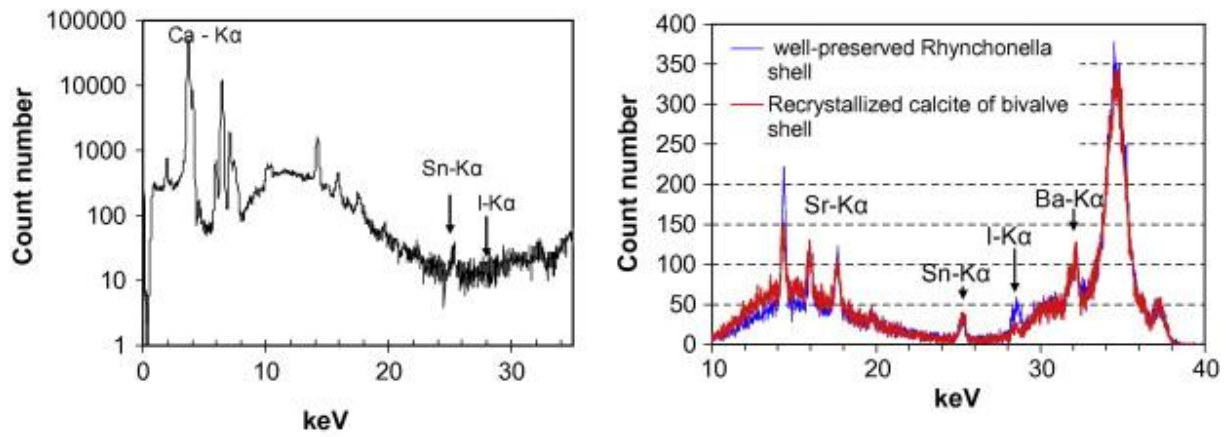
Fig. 4. : On the left, µ-XRF spectrum of Rhynchonella bio-calcite collected with the Si-drift detector showing the difficulty to identify the iodine Kα peak. On the right, comparison of µ-XRF spectra of Rhynchonella bio-calcite and of recrystallized calcite in the bivalve collected using the Si(Li) detector with a 400 µm Al-filter and a collection time of 10 s.